Engineering Structures 65 (2014) 52–61

Contents lists available at ScienceDirect

Engineering Structures

journal homepage: www.elsevier.com/locate/engstruct

# Joints and wood shear walls modelling I: Constitutive law, experimental tests and FE model under quasi-static loading

J. Humbert [a], C. Boudaud [b], J. Baroth [c,*], S. Hameury [d], L. Daudeville [c]

[a] Korea Forest Research Institute, Seoul, Republic of Korea
[b] LUNAM Univ., Groupe Ecole Superieure du Bois, Nantes, France
[c] UJF-Grenoble 1, Grenoble-INP, CNRS UMR 5521, 3SRLab, Grenoble F-38041, France
[d] Centre Scientifique et Technique du Bâtiment, Marne-la-Vallée, France

ARTICLE INFO

*Article history:*
Received 18 June 2013
Revised 14 January 2014
Accepted 29 January 2014

*Keywords:*
Timber-frame structures
Shear walls
Finite element
Cyclic loading
Constitutive law

ABSTRACT

This study is the first of two companions papers that present a finite element (FE) model of timber-frame structures. It introduces a versatile hysteretic constitutive law developed for various joints with steel fasteners commonly used in timber structures (nails, screws, staples, bracket-type 3D connectors, punched plates). Relative to previous models available in the literature, the proposed model improves numerical robustness and represents a step forward by taking into account the damage of joints with metal fasteners. More than 300 experimental tests are carried out on joints and used to calibrate the constitutive law for nails and bracket-type 3D connectors. An average calibration method is presented to take into account the experimental variability. 14 experimental tests are performed on different configurations of shear walls and are used to validate the proposed FE model. Both monotonic and reversed cyclic loadings are used in these quasi-static tests. The FE model predictions are in good agreement with the experimental results. The second paper will present dynamic experiments and numerical predictions of the tests, as well as the development and validation of a computationally efficient simplified modelling of timber-frame structures based on a simplified finite element model for shear walls.



## 1. Introduction

This paper is motivated by two facts. First, timber-frame construction is an increasingly common building system in Europe, primarily for residential single or two-story houses. These structures present many qualities, including good earthquake resistance due to the excellent strength-to-density ratio of timber and to the ductility of joints with metal fasteners, providing limited inertia forces and good energy dissipation, respectively. Second, the most recent European code for the design of earthquake-resistant buildings (Eurocode 8 [15]) has been accompanied by a new seismic hazard map in some countries. Generally, based on these revised maps, earthquake resistance calculations are now mandatory in a lot more cases and the design ground accelerations are greater than previously. Therefore, the seismic behaviour of timber-frame structures must be studied, to better understand their global and local behaviours. This study focuses on shear walls, as they contribute the most to the energy dissipation of structures.

The work presented in these papers is based on a coupled experimental/FE modelling approach. One should note that the behaviour of shear walls can also be estimated through an analytical approach [26,21], but such a method would not allow the analysis of both the global and local behaviour of a timber-framed structure. Therefore, in this study, quasi-static experimental tests on metal fasteners (nails, bracket-type 3D connectors and punched plates) are performed to calibrate their hysteretic constitutive behaviour. Quasi-static and dynamic tests on shear walls are carried out to validate the numerical model for shear walls. Because nonlinear dissipative phenomena in timber-frame structures are mainly concentrated in joints, simplified force–displacement models for joints can be derived from refined analytical or FE models [7,10,1,32,35] or by fitting the results of tests performed on joints [30]. The proposed approach is based on a multi-scale concept, as proposed previously by various authors [38,18,42,36]. Such an approach requires a behaviour law to represent the force–displacement evolution on each scale. Numerous constitutive laws have been developed over the years, from the nonlinear laws for monotonic loads [20,22,27] to hysteretic models of various complexities

* Corresponding author. Address: 3SR Laboratory, Domaine Universitaire, BP53, 38041 Grenoble Cedex 9, France.
*E-mail addresses:* jerome.humbert@gmail.com (J. Humbert), clement.boudaud@ecoledubois.fr (C. Boudaud), jbaroth@ujf-grenoble.fr (J. Baroth).

http://dx.doi.org/10.1016/j.engstruct.2014.01.047
0141-0296/

[8,39,28,40,6,11,17,43,33]. Henceforth, only the hysteretic laws capturing a damage process are discussed. Richard et al. [38] proposed a strength reduction based on a cumulative factor calculated in one direction in respect to the previously achieved strength in the opposite direction. Collins et al. [9] defined a quite similar damage process. Although most of these constitutive laws use exponential functions for the pre-peak backbone curve and hysteresis loops, the model of Ayoub [3] is defined with trilinear functions, in this model the damage process is described in detail and can be divided into four degradation phenomena: strength reduction, unloading stiffness decrease, accelerated stiffness decrease and cap degradation. The evolutionary parameter hysteretic model (EPHM) proposed by Pang et al. [37] is only defined by exponential functions (pre and post-peak backbone, unloading and loading hysteretic loops) and damage is not cumulative. The latest version of the Bouc-Wen-Baber-Noory (BWBN) model has been presented by Xu and Dolan [42]. The BWBN model is analytical and phenomenological. Its history-dependent stiffness and strength degradation provide accurate fitting of reversed-cyclic experimental tests on nailed connections and shear walls, but the BWBN does not rely on physical parameters such as displacements, forces and stiffnesses. A new model, developed by Humbert [23], can be considered an improvement of the Richard et al. [38] and Yasumura et al. [43] models and fulfils the following needs:

- Richard's behaviour law shows that for some sets of parameters (*e.g.* for a metal punched plate), an exponential function does not provide a strict analytical continuity at one end of the branch leading to numerical issues [23]. This issue is shared by all models using the exponential functions originally introduced by Foschi [20].
- The law should model asymmetric behaviour, such as that of punched metal plates for roof trusses and bracket-type 3D connectors. To the best of our knowledge, all of the aforementioned behaviour laws would require new developments to meet this need.
- For the reliability analysis of structures, it is convenient to develop a robust model defined by physical parameters such as displacements, forces, and stiffnesses, whose variabilities can be identified. Although most of the models already meet this condition, the BWBN model does not.

It is important to notice that the hysteretic behaviour of nailed wood joints governs the response of many wood systems when subjected to lateral loadings; the force–displacement backbone and hysteresis curves of shear walls and joints are then similar in shape. Thus, a common feature to all the abovementioned force–displacement models is that they can be used to describe the constitutive behaviour of joints as well as the global shear wall response to lateral forces.

In this study, a new hysteretic constitutive behaviour law for joints and timber-frame structures is proposed, and its application to the modelling of oriented strand board (OSB) and particleboard sheathed shear walls is presented. More than 260 tests on nailed joints and 50 tests on connections made with bracket-type 3D connectors are performed. The calibration of the law at the joint scale is detailed, and particular emphasis is given on how to take into account the variability of the experimental results. Tests performed on 7 different configurations (combining different specimens and vertical loadings) of shear walls are described. The development of the numerical model of shear walls is then explained. To assess its capability to predict the behaviour of different configurations of shear walls, its predictions are compared to the experimental results of the 14 tests under quasi-static loading. Experimental tests present a certain variability and the large sample size allows its quantification. Then, when comparing the deterministic predictions of the model to the experimental results, the experimental variability can be considered. Moreover, tests on different configurations are designed to estimate the model versatility.

## 2. Force–displacement hysteretic constitutive law

The one-dimensional constitutive law is shown in Fig. 1.

The following notations are used to describe the asymmetric feature of the modelled systems and the notion of force sign. The $\square^+$ direction corresponds to the first direction of loading in the case of reverse loading ($\square^-$ refers to the opposite direction). In the absence of a superscript, the parameters refer to both sides

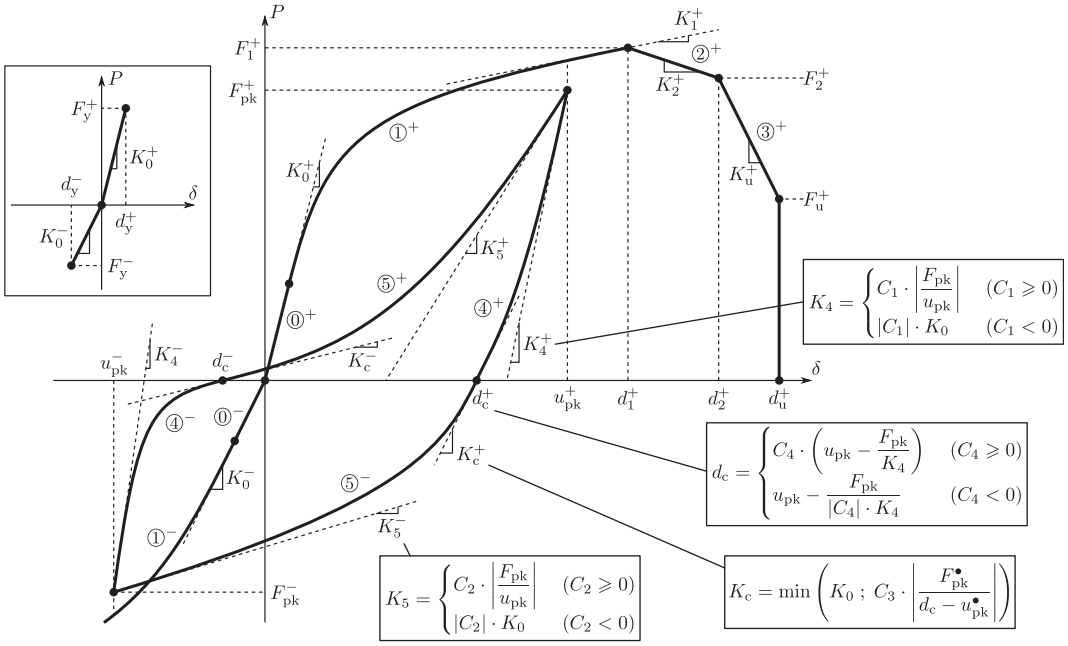


**Fig. 1.** Proposed force–displacement constitutive law [23].

**Table 1**
Model parameters governing the constitutive behaviour under monotonic loading.

| Parameter | Unit | Description |
|---|---|---|
| $K_0$ | N/m | Initial elastic stiffness |
| $d_y$ | m | Yield limit |
| $d_1$ | m | Displacement at peak force |
| $F_1$ | N | Peak force |
| $K_1$ | N/m | Pre-peak tangent stiffness |
| $d_2$ | m | Intermediate displacement limit |
| $F_2$ | N | Force at intermediate limit $d_2$ |
| $d_u$ | m | Ultimate displacement |
| $F_u$ | N | Force at ultimate displacement |

of loading. A bullet superscript $\square^\bullet$ is used to refer to the side opposed to the implied one. For example, $a = b^\bullet$ implies that $a^- = b^+$ and $a^+ = b^-$. The branches of the force-displacement model are grouped into two distinct categories and numbered from (0) to (5). A first group, formed by branches (0) to (3), describes the behaviour under monotonic loading. The initial linear branch (0) ranges from the zero displacement up to the yield displacement $d_y$. The corresponding elastic stiffness is $K_0$. This branch is followed by branch (1), which models the nonlinear phenomena in the joint up to the force peak at $(d_1, F_1)$. After the force peak, branches (2) and (3) model up to the ultimate displacement $d_u$ at force $F_u$ associated with the collapse of the joint. $F_u$ is generally chosen to be null to ensure a correct continuity of forces and prevent numerical issues. This first set of 9 parameters is summarised in Table 1. These parameters are similar to those proposed by Richard et al. [38]. Branch (1) is defined using a rational quadratic Bézier curve, replacing the original exponential function introduced by Foschi [20] and providing a strict analytical continuity of forces.

A second group of branches describes the hysteresis loops typically observed when the joint undergoes a reversed loading. To describe these branches, the $\square_{max}$ subscript is defined, which corresponds to the absolute maximum value reached over the past loading history up to the current time step. Additionally, the $\square_{pk}$ subscript corresponds to the value at the last loop peak. Starting from a previously reached loop peak $(u_{pk}, F_{pk})$, branch (4) models the nonlinear elastic unloading down to a null force. A residual displacement $d_c \neq 0$ is commonly observed due to prior plastic deformations. The unloading stiffness $K_4$ is either (a) proportional to the elastic stiffness $K_0$ of the joint or (b) proportional to the secant stiffness $F_{pk}/u_{pk}$ when modelling a stiffness decrease with displacements of increasing amplitude. Examples of (a) and (b) include cases in which the overall behaviour of the joint is dominated by the embedment of wood dominating and by the pulling-out of the fastener from the timber members and/or the plastic yielding of the fastener, respectively. Following this unloading, loading in the opposite direction is modelled with branch (5). The stiffness at $d_c$ between branches (4) and (5) is denoted by $K_c$ and is used as a tangent for both branches for the sake of continuity. Branch (5) eventually reaches the previous loop peak $(u^\bullet_{pk}, F^\bullet_{pk})$ in the opposite loading direction. Like the unloading stiffness $K_4$, the reloading stiffness $K_5$ is proportional to the elastic stiffness $K_0$ or the secant stiffness $F_{pk}/u_{pk}$. A second set of 4 control parameters $C_{i=1,\dots,4}$ governs the shape of the hysteresis loops, allowing the modelling of several mechanical behaviours, *e.g.*, the adjustment of the thickness of the pinching area. Parameters $C_1$ and $C_2$ control the unloading stiffness $K_4$ and reloading stiffness $K_5$, respectively. Parameter $C_3$ controls the tangent stiffness $K_c$ at location $(d_c, 0)$. Values of $C_3$ greater than 1 model a thick pinching area, while values less than 1 model a thin pinching area. A physical limitation is also imposed so that $K_c$ cannot exceed the initial elastic stiffness $K_0$. Finally, parameter $C_4$ controls the value of the residual displacement $d_c$ after the nonlinear elastic unloading. Based on observations from experimental tests, this displacement can be related to the fictive residual displacement $u_0 = u_{pk} - F_{pk}/K_4$ after a hypothetical *linear elastic* unloading with stiffness $K_4$ from $(u_{pk}, F_{pk})$. Alternatively, for some other cases, $d_c$ is related to the residual displacement after a linear elastic unloading with a stiffness $|C_4| \cdot K_4$ proportional to the secant stiffness. These control parameters $C_{i=1,\dots,4}$ (Table 2) mainly depend on the phenomena involved, and therefore on the configuration of the modelled system. They are constant for a given configuration.

**Table 2**
Model parameters governing the shape of hysteresis loops.

| Parameter | Unit | Controls |
|---|---|---|
| $C_1$ | – | Unloading stiffness |
| $C_2$ | – | Reloading stiffness |
| $C_3$ | – | Tangent stiffness at $F = 0$ |
| $C_4$ | – | Residual displacement |

Lastly, a third set of 3 parameters controls the damage process of the model. The word *damage* refers here to the decrease in strength under cyclic loading. It is based on the hypothesis that the hysteresis loops are bound by the backbone curve, which models the force-displacement evolution of the joint under monotonic loading. During the first loading, the peak $(u_{pk}, F_{pk})$ is located on the backbone curve. The damage process defines the evolution of the ratio (1-$D$) between the "nondamaged load" $F_{mono}$ and the "damaged load" $F_{pk}$. The scalar damage indicator $D$ ranges from 0 to 1, where $D = 0$ corresponds to a nondamaged mechanical system and $D = 1$ corresponds to a fully collapsed mechanical system. $D$ is increased by $\Delta D$ at each change of the force sign ((4) to (5) in Fig. 1). To ensure the damage stabilisation after a few cycles of constant amplitude occurs as experimentally observed, the increment $\Delta D$ is defined as $\Delta D = \eta(D_\infty - D)$, where $\eta$ defines the proportion of damage at constant amplitude cycles and $D_\infty$ is an upper limit of $D$ for the displacement $d_{max}$. This limit is constant for a given maximum displacement $d_{max}$. $D_\infty$ is defined by Eq. (1) as a function of $d_{max}$ using a power law. This function is referred to as the "damage limit function (DLF)". A power term $B_r > 1$ ensures that the damage remains moderate before the force peak and becomes severe after the peak. This model is consistent with experimental observations. Table 3 summarises the three damage parameters.

$$D_\infty = B_c(d_{max}/d_1)^{B_r} \tag{1}$$

## 3. Scale 1: Joints with metal fasteners

In this section, quasi-static experimental tests carried out on joints with metal fasteners are presented. Then, the calibration of the parameters of the constitutive law of joints is described.

### 3.1. Experimental tests

Experimental tests on joints with metal fasteners (scale #1) are conducted to provide input data for the numerical model of the shear wall (scale #2). There are three different steel joints in a shear wall:

- Panel-to-frame (P2F) joint: In this study, these joints are made with nails. Fig. 2a shows a nail after a shear wall test. Only ring shank and square masonry nails are used, as it is common in

**Table 3**
Parameters governing the damage indicator calculation.

| Parameter | Unit | Description |
|---|---|---|
| $B_c$ | – | Linear coefficient of the DLF |
| $B_r$ | – | Power term of the DLF |
| $\eta$ | % | Damage proportion at constant amplitude cycles |

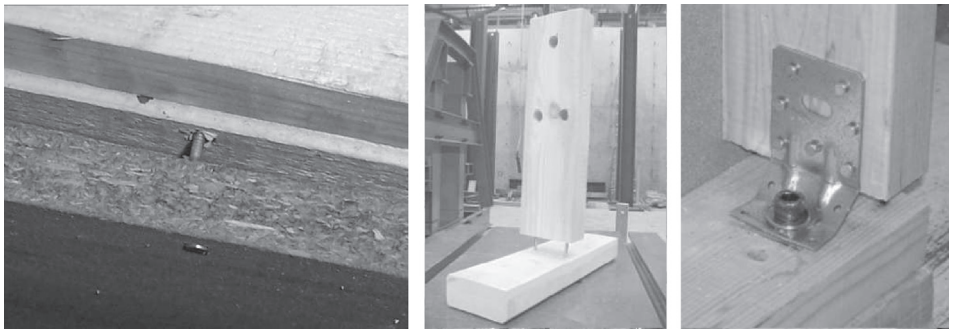

(a) Panel-to-frame nail joint (b) Frame-to-frame nail (c) Frame-to-frame bracket

**Fig. 2.** Photographs of the three joints with metal fasteners used in a shear wall.

France. Their dimensions ranges from 2.1 mm to 3.1 mm in diameter and 45 mm to 90 mm in length. Electrogalvanization and hot-dip galvanizing coatings, as well as stainless steel are used.

- Frame-to-frame nail (F2F nail): The joints between the top/sill plate and the studs are composed of 3 to 5 nails. Their usual length is approximately 90 mm for a diameter of 3.1 mm. Fig. 2b presents such a connection after a pull-out test.
- Frame-to-frame bracket (F2F bracket): At both ends of the shear wall, the F2F connections must be strengthened to prevent uplift of the exterior studs. Thus, an additional bracket-type 3D connector is used. Fig. 2c displays a F2F bracket joint at the end of a shear wall test. The 3D connector is connected by an anchor or bolt to the foundation or the lower story.

Thirty-three configurations of P2F nail connections are tested, 3 of which are used in the 3 tested configurations of shear walls considered in this study: 9 and 12 mm OSB with 2.1 × 45 mm nails and 16 mm particleboard with 2.5 × 50 mm nails, respectively named OSB9, OSB12 and P16. The wood member dimensions are 45 × 115 × 250 mm. Fig. 3a shows the principle of these tests, which consists of a shear test, first under a monotonic loading and then under reversed-cyclic loading (EN 12512 [13]). The grain orientation of the wood member and the orientation of the panel are not variable parameters of the tests, based on the results presented by [19] for parallel and perpendicular to grain tests on nail joints. The high number of configurations and the repeated tests per configuration led to a total of 263 tests for P2F nail joints. F2F nail joints were not tested and the results of tests achieved by Richard et al. [38] are used instead. These tests (Fig. 3b) consist of a cyclic pull-out load on a joint. The same tests are performed on F2F joints made of bracket-type 3D connectors only (Fig. 3c). In that case, wood member dimensions are 45 × 140 × 400 mm. For

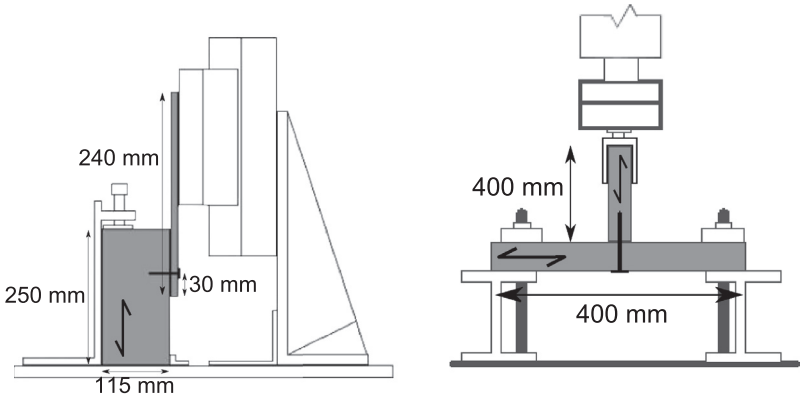


(a) Panel-to-frame (b) Frame-to-frame nail

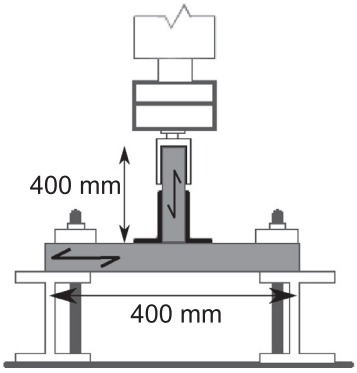


(c) Frame-to-frame bracket

**Fig. 3.** Experimental tests on metal fastened joints.

each configuration, the tests were repeated twice for monotonic loading and 5 times for reversed cyclic loading, which led to a total of 56 quasi-static tests.

Although it is not the main concern of this paper, some results of the experimental tests are provided herein. For each monotonic test, the yield displacement $V_y$, the ultimate displacement $V_u$ (from which the ductility is derived $D_s = V_u/V_y$), the maximal force $F_{max}$ are calculated according to the Equivalent Energy Elastic–Plastic (EEEP) method [2].

For the nail connections, the failure mode according to Johansen's theory [24] (only one or two plastic hinges, because no wood crushing modes were observed) and the ultimate failure mode (withdrawal of the nail shank or pulling through of the nail head) are also provided. Three monotonic tests are performed for each configuration of nail joint and Table A.5 presents the average results. The EEEP method provides consistency in the $V_y$ calculation method but, as it has been show by Munoz et al. [34] and confirmed by Malo et al. [31], is hardly satisfying for some tests results. Moreover, the values of $V_y$ greatly affects the static ductility $D_s$ and explain why it reaches unexpected values, such as 43 for configuration N15. Under monotonic loading the dominant mode of failure is the pulling through of the nail head. Withdrawal of the nail shank is also observed, it is generally partial and becomes a failure mode for smaller nails dimensions. As expected, it is observed that smaller diameters tends to fail with two plastic hinges, indeed this failure mode only happens for diameter equal or inferior to 2.3 mm. It is also confirmed that the two plastic hinges failure mode leads to greater values of ductilities. The Fig. 4a shows a typical force–displacement evolution of a nail connection. It is obvious that damages due to the cyclic loading reduces the maximal force $F_{max}$ (by 20% in average) and the ultimate displacement $V_y$.

For the bracket connections, the failure modes are complex as they include the nails behaviour under shearing and strict withdrawal loading, the bracket folding or unfolding and wood crushing. For that reason, the results of the 3D bracket tests presented in Table A.6 are limited to the values of $V_y$, $V_u$, $D_s$ and $F_{max}$. The Fig. 4b displays a typical force–displacement evolution of a single bracket specimen in the $Y$ direction. In that case, the joint is stiffer in $Y-$ as it corresponds to the wood compression, while $Y+$ only correspond to the unfolding of the bracket. In average, the maximal force $F_{max}$ under cyclic loading is 15% smaller than under monotonic loading, and the ductility is reduced by 32%.

### 3.2. Calibration of the force–displacement model

The results of the tests achieved on P2F nails are used to calibrate the constitutive model. Two levels of calibration are distinguished: the first level is a direct calibration, which consists of reproducing one particular test, and the second level is an average calibration, which consists of calibrating the parameters to reproduce the average behaviour observed in several experiments. The hysteretic model is based on three types of parameters: backbone curve (Table 1), pinching (Table 2), and damage (Table 3). Fig. 5a presents a direct calibration of parameters for a P2F nail joint. This calibration is achieved by calculating the backbone curve parameters from a single test under monotonic loading and calibrating the pinching and damage parameters by successive simulations. The average calibration is based on the observation that backbone curve parameters display some variability, while the pinching parameters do not. Using the direct calibration as a starting point, the backbone curve and damage parameters are re-calibrated so that the simulation now reproduces the average envelope curve of all available cyclic tests. Fig. 5b presents the average envelope curve and the calibrated model. This process provides the joint models used in the subsequent shear wall modelling.

It is worth noticing that, in Fig. 5a, the force–displacement curve under reversed cyclic loading is asymmetric. The resistant forces are greater in compression (when the panel moves downward, see Fig. 3a). It is believed that the asymmetry of the timber assembly and slight misalignments of the test machine induce more friction in compression. This phenomenon was also observed by Fonseca et al. [19] and Li et al. [29], who present experimental tests on similar connections (panel to stud with only one nail). Li et al. [29] explain this behaviour by the fact that wood and metal damages on one side also affect the strength on the other side. However, although the tests described in this study were conducted by loading first in traction and then in compression, the forces were greater in compression, not in traction. It is then believed that the phenomenon described by Li et al. [29] does not have a significant effect relative to the friction phenomenon we described. This point is further discussed later in this study for tests on shear walls. As the loading conditions of the joint tested are not strictly similar to the conditions for P2F connections in the full size shear wall, neither in compression nor in traction, the calibration is achieved on the average behaviour between compression and traction.

Fig. 6a shows the numerical behaviour of a F2F nail joint in pull-out and compression. The compression (contact between the two timber elements) is linear and the stiffness is calculated according to the material characteristics and the dimensions of the section in contact. The pull-out behaviour is bilinear, and the parameters are estimated from tests carried out by Richard et al. [38]. The shear behaviour is linear and symmetric. The stiffness is calculated according to Eurocode 5 [14]. Note that for all joints (P2F and F2F), no rotational stiffness is implemented. For F2F joints, it is

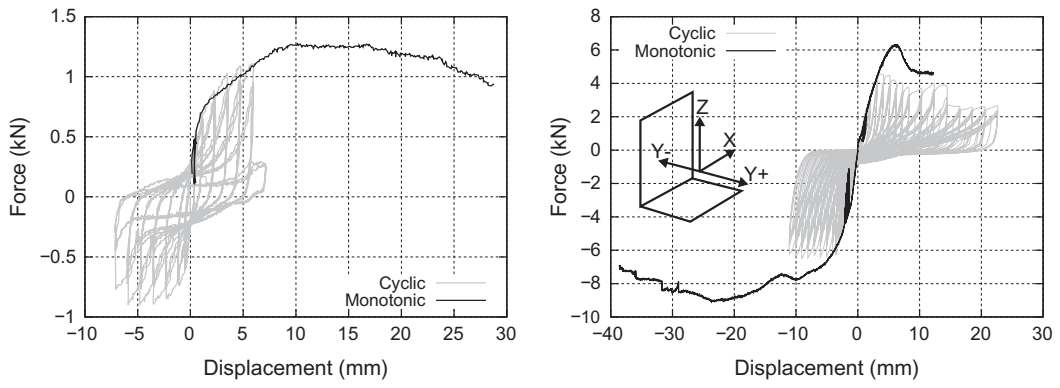


(a) Nail (Test N17) (b) 3D Bracket in the Y direction (Test B3)

**Fig. 4.** Typical monotonic and cyclic force–displacement evolutions for nail and 3D brackets connections.

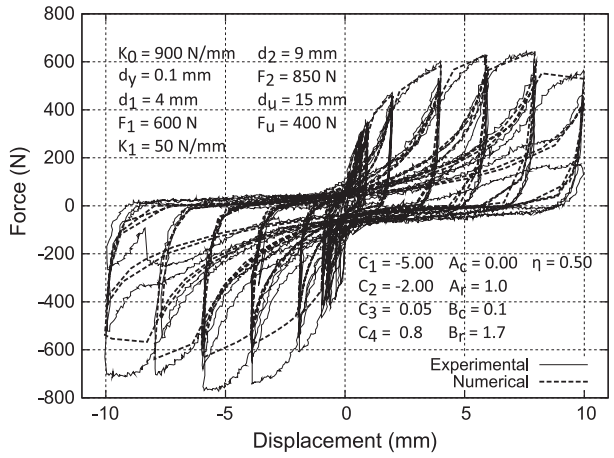


(a) Direct calibration

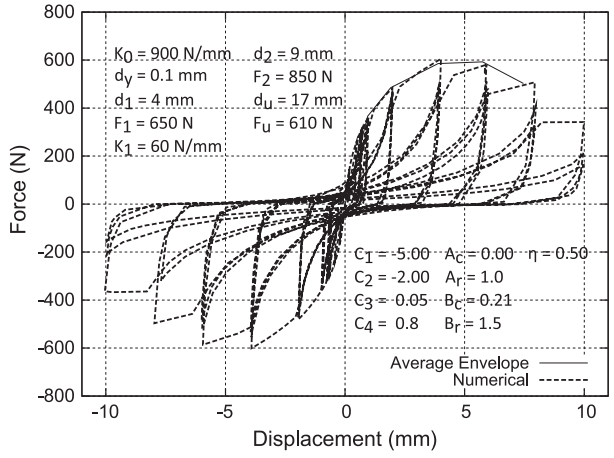


(b) Average calibration

**Fig. 5.** Calibration of the hysteretic model for a 2.1 mm × 45 mm P2F nail in a 9 mm OSB panel.

justified by the fact that their rotational stiffness is insignificant compared to the stiffness provided by the sheathing panels.

Fig. 6b shows the numerical behaviour of a F2F bracket joint with an E5® bracket-type 3D connector in pull-out and compression. This combination behaves the same in compression as the F2F nail joints. Experimental tests were carried out on E5® connectors in shear and pull-out. In contrast, the behaviour of joints made with AH connectors was estimated based on the connector properties and set as bilinear. Shear behaviour is linear and symmetric. The E5® pull-out behaviour parameters are calibrated using the same method as P2F connections.

## 4. Scale 2: Shear wall

In this section, quasi-static experimental tests carried out on shear walls are presented. Then, numerical modelling of timber framed shear walls is detailed. Finally, the predictions of the FE model of shear wall are confronted to the experimental results.

### 4.1. Experimental tests

The shear walls studied in this study correspond to structural elements found in conventional timber-framed houses in Europe, which are quite similar to typical North American shear walls, except for the nail diameter of the P2F joints. The diameter of these nails rarely exceeds 3 mm in France (common dimensions are between 2.1 mm and 2.5 mm) while it is generally greater than 3 mm in America. Fig. 7 describes the shear wall technology and its dimensions. The frame is made of C24 timber (strength class according to the European standard EN 338 [16]). To provide shearing resistance, wood-based panels are nailed to the frame. These panels are usually OSB, particleboard or plywood. In this study, OSB-3 panels and P5 particleboards are used (panels classification according to EN 12369-1 [12]). The P2F joints can be formed with nails, screws, or staples. The spacing between two P2F joints along the perimeter of the panel is set to 150 mm ($s_{ext}$) and 300 mm ($s_{int}$) along intermediate studs. The connections between horizontal frame elements (sill or top plates) and vertical frame elements (studs) are formed with long nails (3.1 mm × 90 mm in this study). The anchorage of the shear walls – on the foundation or the lower story – is achieved with bolts. Current anchorages refer to regularly settled bolts, one in every span between two studs. Their purpose is to transfer the shearing load. Exterior anchorages refer to the addition of a 3D connector affixed to the exterior stud and a bolt. Their purpose is to transfer the vertical uplifting loads. Two 3D bracket-type connectors are used, both provided by Simpson Strong-Tie®: E5® standard and AH2950/2® reinforced connectors (referred to as AH). AH brackets are specifically designed to withstand high uplifting loads.

The experimental tests on shear walls are detailed in Boudaud et al. [4]. Fig. 7 displays the principle and protocol (EN 12512 [13]) of the tests. OSB9, OSB12, and P16 configurations of shear walls are tested. One push-over and two reversed-cyclic tests were achieved for each configuration tested. Maximal forces for cyclic tests can be seen on Table 4.

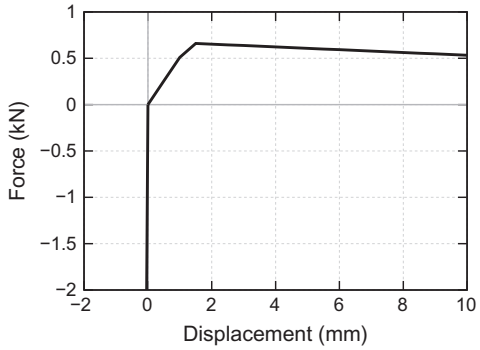


(a) F2F nail: pull-out and compression

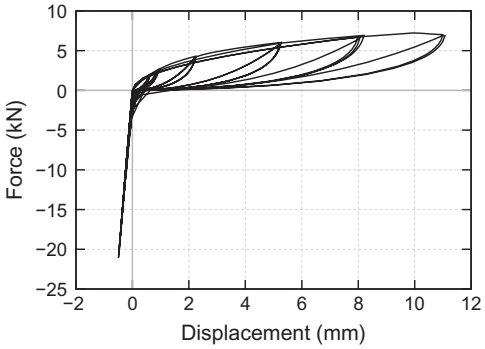


(b) F2F bracket (E5®) connector: pull-out and compression

**Fig. 6.** Behaviour law for Frame-to-frame joints.

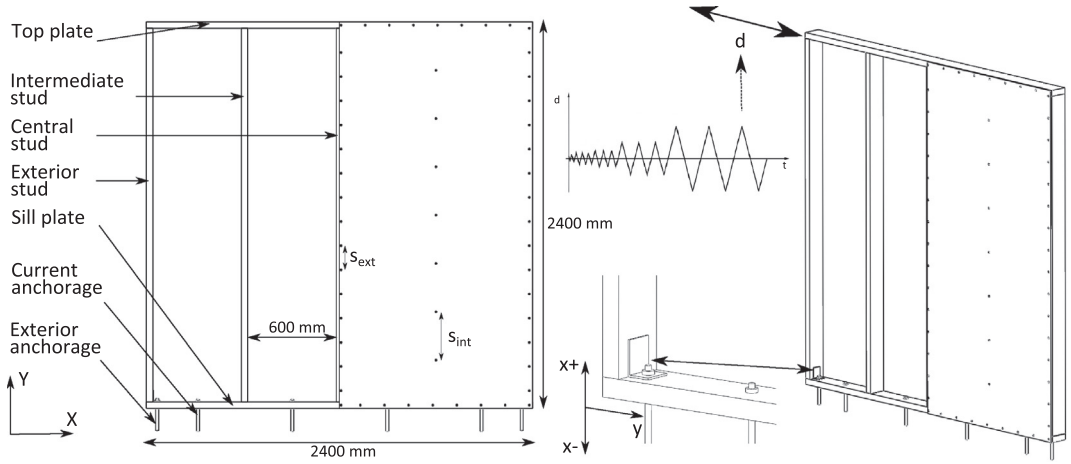


**Fig. 7.** Shear wall description and principle of reversed cyclic tests.

**Table 4**
Experimental and numerical comparison for reversed-cyclic loading.

| Configuration | | | | Results | | | |
|---|---|---|---|---|---|---|---|
| Panel | F2F Angle | P2F ($\varnothing \times L$) | Vertical load (kN) | $F_{max}$ (kN) Exp | Num | $\Delta$ (%) | Ref. |
| OSB9 | E5 | 2.1 × 45 | 0 | 12.0 | 11.7 | +2.5 | SW1 |
| | | | | 12.2 | | +4.1 | SW2 |
| | | | 5.5 | 11.9 | 11.3 | +5.3 | SW3 |
| | | | | 12.7 | | +3.4 | SW4 |
| OSB12 | E5 | 2.1 × 45 | 0 | 12.1 | 11.8 | +2.2 | SW5 |
| | | | 6 | 13.2 | 13.0 | +1.7 | SW6 |
| | AH | 2.5 × 50 | 3 | 12.4 | 13.7 | −10 | SW7 |
| | | | | 14.0 | | +1.5 | SW8 |
| P16 | E5 | 2.5 × 50 | 6 | 14.2[a] | 14.8[a] | −3.7[a] | SW9 |
| | | | | 18.7 | 18.8 | −0.38 | SW10 |
| | AH | | 0 | 23.2 | 20.9 | +10 | SW11 |
| | | | | 23.4 | | +11 | SW12 |
| | | | 3 | 22.0 | 20.8 | +5.4 | SW13 |
| | | | | 22.9 | | +8.9 | SW14 |

[a] For this shear wall $s_{ext} = 300$ mm along the central stud (instead of 150 mm).

### 4.2. Numerical modelling

The finite element modelling of shear walls was conducted using beam, plate, and two-node spring-like finite elements. The constitutive behaviour presented previously was implemented using the free software Code_Aster.[1] Fig. 8 presents a schematic view of the finite element model of a shear wall. Euler beam elements model the frame, and their elastic modulus and density are the mean values corresponding to C24 timber according to EN 338 [16] provisions. Four-node plane stress elements model the panels, and their material properties are isotropic and correspond to OSB-3 or P5 according to EN 12369-1 [12] provisions. Each two-node spring-like element models a metal fastener joint whose properties are given by the previous calibration. The resulting mesh is composed of 108 P2F, 8 F2F nail and 2 F2F angle elements. The F2F joints have different behaviours in shear and pull-out/compression: therefore, each behaviour law is affected to the corresponding translational degree of freedom (DOF). For each P2F connection, a local basis is oriented according to the relative displacement direction, and the constitutive law is affected to both translational DOF in this basis. Richard et al. [38] showed that this direction is globally constant over the calculation. Judd [25] developed an oriented spring pair model based on this observation. As the drift direction is not strictly constant, its change over the calculation has been quantified by calculating the ratio $F_y/F_x$ ($F_x$ and $F_y$ are the forces associated with the translational DOFs of the element in the local basis). This ratio is less than 0.3 for 80–90% of the P2F connections. As a result,

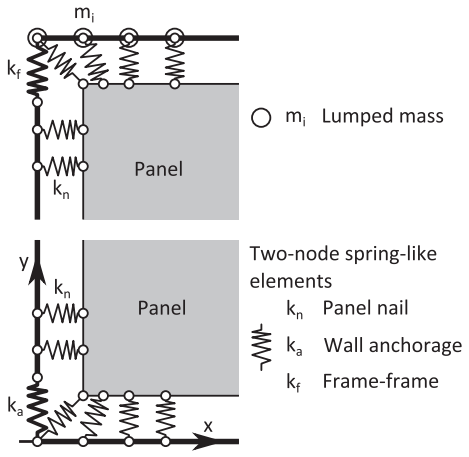


**Fig. 8.** Finite element modelling of a shear wall.

[1] All documentation available at www.code-aster.org.

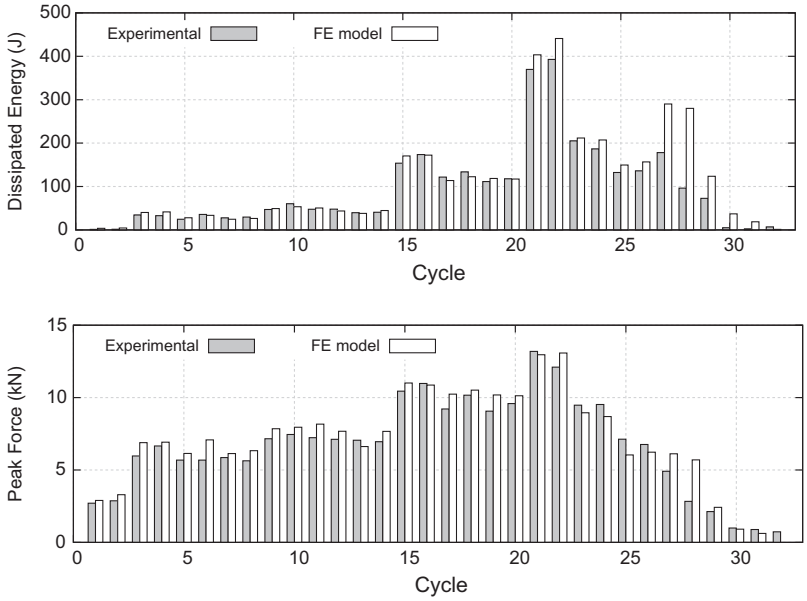


**Fig. 9.** Dissipated energy and peak forces: comparison between the experimental results and FE model predictions.

the effect of the overestimation of the resistance of the joints is insignificant at the scale of the wall.

The sill plate is considered to be embedded because insignificant displacements are recorded in tests. The top plate and the highest node of each external stud undergo an imposed displacement. To comply with the experimental set-up, as the actuator pushes a metal plate attached to the wood top plate and the top of the external studs. Experimentally, a vertical load is applied to the shear wall in approximately half of the tests (6 kN on each stud). The global responses show very limited influence of the vertical load. Nevertheless, the uplift of the external studs is affected by the vertical load. With loading, no uplift is observed. Without loading, the uplift of exterior studs is significant, and the 3D connectors are strained beyond their yield limit. Numerically, a vertical load can be applied to the model. In that case, the load is uniformly distributed along the plate.

### *4.3. FE model predictions vs. experimental results*

The model predictions are compared to 14 experimental results obtained from quasi-static tests under reversed-cyclic loading. Thus, the numerical predictions can be compared to several configurations of shear walls (different nails, sheathing panels and vertical loading conditions). Moreover, two tests are performed for each configuration, which limits the effects of the variability when comparing the experimental behaviour to the numerical predictions. Table 4 presents the results in terms of peak forces. It shows that the peak forces predicted by the numerical model are in good agreement with the experimental results.

To assess the quality of the model predictions, the dissipated energy is often used [5,9,37,41]. This approach consists of calculating the areas inside the hysteresis loops, but similar values do not necessarily mean that both force–displacement evolutions are equivalent. As a result, the area and peak force of each half-cycle should be compared simultaneously to assess the similarity between experimental and numerical hysteresis loops. Fig. 9 presents such a comparison for one of the tests (OSB12 C2), showing that the detailed FE model is able to predict the peak force and the area inside the hysteresis loops, and therefore their shapes, fairly accurately. It also shows that the errors of the FE model predictions are more significant for the last few cycles. Nevertheless, authors point out that the same observations can be made from the force–displacement comparison presented in Fig. 10a, for the same test. Fig. 10b compares the experimental and calculated force–displacement curves for the OSB9 shear wall. From the two examples of predictions presented in Fig. 10, and the results presented in Table 4, it can be seen that the model predictions are in good agreement with the experimental behaviour. Indeed, the pinching and

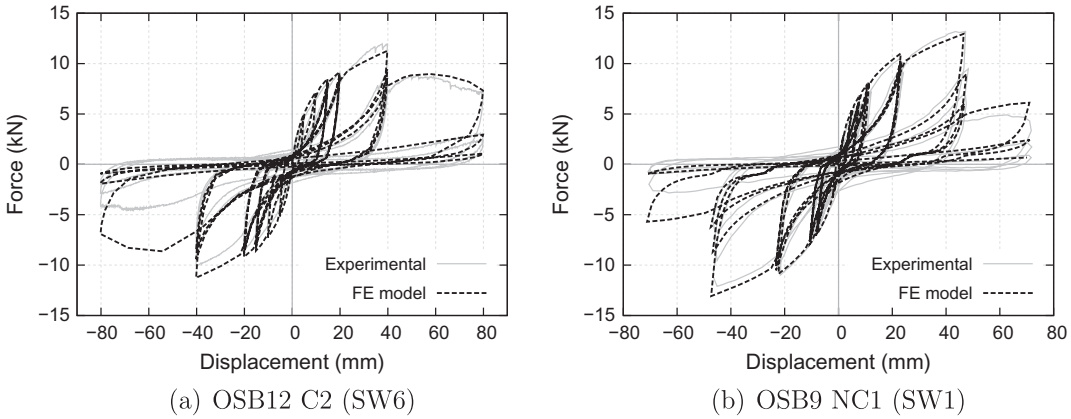


**Fig. 10.** Force–displacement curves of shear walls: comparisons of experimental results and FE model predictions.

peak forces of the hysteresis loops are in accordance with the experimental data. Fig. 9a and b also show that the last cycle in the negative side is over predicted. Experimentally, this cycle is clearly asymmetric in terms of force, which is explained by the fact that the failure of the wall occurs during this cycle. Therefore, these over predictions are not considered to be an issue, because the model is "only" intended to predict the behaviour up to the failure.

One should note that the error estimation between experimental and numerical hysteretic curves equally concerns the constitutive law calibration at scale 1 and the detailed FE model predictions at scale 2 presented herein. In this study, errors quantification has not been used, as the quality of the numerical predictions (Table 4) were considered to be satisfactory.

Like nails, shear walls present a strength asymmetry. For nails, this behaviour is believed to be due to the asymmetry of the wood assembly. This cannot be the case for shear walls because they are, like the test machine, symmetric. Moreover, a comparison of the nail and shear wall results (Figs. 5a and 10, respectively) show that the behaviours are quite different. For nails, the asymmetry is significant at all magnitudes, whereas it appears to increase with the cycle magnitude in the case of shear walls. This can be explained by the phenomenon described by Li et al. [29] (page 12). In conclusion, it is believed that the two phenomena can induce a strength asymmetry. For tests on asymmetric joints, the effect of friction is dominant, while the effect of damage prevails for tests on symmetric elements.

## 5. Conclusion

This study is dedicated to the development of a versatile hysteretic constitutive behaviour law for timber joints made of metal fasteners. The main features of the model are its ability to accurately describe the hysteretic behaviour, notably by considering the damage effects (strength reduction), and its numerical robustness compared to existing models using exponential functions.

In the second part of this study, the results of more than 300 tests performed on timber joints with metal fasteners show a significant variability. An average calibration method is thus developed for the identification of the model parameters. Using these calibrated models of joints, a FE model of a shear wall is developed. The frame is modelled by Euler beams elements, the panels by four-node plates elements, and every joint by a two-node spring-like element. The FE model predictions are compared to the results of 14 experimental quasi-static tests for validation. These comparisons show that the FE model accurately predicts the experimental behaviour of different configurations of shear walls.

In part II of these two companions papers, dynamic experimental tests and numerical calculations are addressed, and a simplified FE model of shear wall is presented. This simplified model is used to build a FE model of the structure.

## Acknowledgements

The SISBAT research project is funded by the French Agency ANR (Agence Nationale de la Recherche ANR-08-RISKNAT2008). Authors would like to express their gratitude for this support and thank the members of this project for their contributions and databases, especially Mrs C. Faye (FCBA Technological Institute) and her colleagues, for the effort provided.

## Appendix A. Experimental data

Tables A.5 and A.6.

**Table A.5**
Experimental results on nail joints (Fig. 3a) for monotonic loading.

| No. | Configuration | | | | Results | | | | | |
|---|---|---|---|---|---|---|---|---|---|---|
| | $\varnothing \times L$ | Shape | Mat | Panel | $V_y$ | $V_u$ | $D_s$ | $F_{max}$ | Mode | Hinge |
| N1 | 2.1 × 38 | RSN | SS | OSB9 | 0.8 | 21.7 | 28.2 | 962 | W | 2 |
| N2 | | | | OSB12 | 1.3 | 21.9 | 22.1 | 934 | W+P | 2 |
| N3 | | | | OSB15 | 0.6 | 15.0 | 26.6 | 734 | W | 2 |
| N18 | 2.5 × 60 | | | OSB9 | 2.1 | 17.5 | 8.4 | 1626 | P | 1 |
| N19 | | | | OSB12 | 2.5 | 21.8 | 8.7 | 1470 | P | 1 |
| N20 | | | | OSB15 | 1.6 | 21.8 | 14.0 | 1142 | P | 1 |
| N25 | 3.1 × 85 | | | OSB9 | 2.2 | 17.5 | 8.1 | 1913 | P | 1 |
| N26 | | | | OSB12 | 2.6 | 22.9 | 9.0 | 1661 | P | 1 |
| N27 | | | | OSB15 | 2.7 | 23.3 | 9.0 | 1293 | P | 1 |
| N4 | 2.1 × 45 | | EG | OSB9 | 1.2 | 15.5 | 15.3 | 855 | P | 1 |
| N5 | | | | OSB12 | 2.3 | 21.1 | 9.9 | 1005 | P | 1 |
| N16 | 2.5 × 50 | | | P10 | 2.8 | 24.1 | 8.8 | 1577 | W | 1 |
| N17 | | | | P16 | 1.1 | 23.2 | 20.9 | 1276 | W | 1 |
| N6 | 2.1 × 45 | | | OSB9 | 1.6 | 15.3 | 9.5 | 925 | P | 1 |
| N7 | | | | OSB15 | 0.7 | 17.3 | 29.2 | 1001 | W+P | 2 |
| N21 | 2.8 × 80 | | | OSB9 | 2.1 | 15.7 | 7.9 | 1525 | P | 1 |
| N22 | | | | OSB15 | 1.3 | 21.6 | 16.9 | 1962 | W+P | 1 |
| N8 | 2.3 × 60 | | HdG | OSB9 | 1.4 | 13.9 | 10.7 | 1153 | P | 1 |
| N9 | | | | OSB15 | 3.4 | 24.2 | 7.4 | 1247 | W+P | 1 |
| N30 | 3.1 × 90 | | | OSB9 | 1.6 | 14.3 | 9.3 | 1244 | P | 1 |
| N31 | | | | OSB15 | 1.8 | 18.1 | 10.3 | 1871 | P | 1 |
| N14 | 2.3 × 60 | SMN | SS | OSB9 | 1.1 | 26.0 | 32.4 | 1013 | P | 2 |
| N15 | | | | OSB15 | 0.8 | 29.6 | 43.0 | 965 | W | 2 |
| N28 | 3.1 × 85 | | | OSB9 | 0.6 | 14.7 | 23.2 | 1797 | P | 1 |
| N29 | | | | OSB15 | 1.0 | 30.1 | 34.8 | 1329 | P | 1 |
| N12 | 2.3 × 60 | | HdG | OSB9 | 1.4 | 13.9 | 10.3 | 1279 | P | 1 |
| N13 | | | | OSB15 | 0.9 | 19.2 | 21.4 | 1629 | P | 2 |
| N23 | 3.1 × 75 | | | OSB9 | 1.2 | 15.9 | 20.8 | 2073 | P | 1 |
| N24 | | | | OSB15 | 1.0 | 18.2 | 18.0 | 1864 | P | 1 |
| N10 | 2.3 × 60 | RSN | | P10 | 2.2 | 24.3 | 11.3 | 2208 | P | 1 |
| N11 | | | | P16 | 2.7 | 32.9 | 12.5 | 1583 | W | 2 |
| N32 | 3.1 × 90 | | | P10 | 1.6 | 20.5 | 13.9 | 2015 | P | 1 |
| N33 | | | | P16 | 2.0 | 23.3 | 12.4 | 2187 | P | 1 |

$\varnothing \times L$: Nail diameter and length in mm. Mat: Nail material. $V_y$ and $V_u$ in mm. $F_{max}$ in N. Mode: Mode of failure. Hinge: Number of hinges. RSN: Ring Shank Nail. SMN: Square Masonry Nail. SS: Stainless Steel. EG: Electrogalvanization. HdG: Hot-dip Galvanising. W: Nail withdrawal. P: Nail pulling through the panel.

**Table A.6**
Experimental results on bracket joints (Figs. 3c and 4b) for monotonic loading.

| No. | Configuration | | | | Results | | | |
|---|---|---|---|---|---|---|---|---|
| | Type | Dir. | Support | # | $V_y$ | $V_u$ | $D_s$ | $F_{max}$ |
| B1 | E5 | X | Wood | 4 | 4.5 | 35.9 | 8.1 | 32.9 |
| B2 | | | Steel | 4 | 3.1 | 31.7 | 10.1 | 19.4 |
| B3 | | Y | Wood | 1 | −2.8 | −41.4 | 14.9 | −9.8 |
| | | | | | 3.8 | 10.9 | 2.7 | 5.8 |
| B4 | | | | 2 | 3.7 | 26.5 | 7.5 | 14.7 |
| B5 | | | Steel | 1 | −3.2 | −28.0 | 8.7 | −14.2 |
| | | | | | 1.3 | 10.6 | 9.0 | 4.5 |
| B6 | | | | 2 | −2.1 | −28.5 | 13.9 | −15.1 |
| B7 | | Z | Wood | 2 | 1.8 | 9.0 | 5.0 | 7.3 |
| B8 | | | Steel | 2 | 3.2 | 19.4 | 6.3 | 18.9 |
| B9 | | XY | Wood | 1 | −12.3 | −50.4 | 4.1 | −11.6 |
| | | | | | 5.5 | 23.0 | 4.2 | 5.5 |
| B10 | | | Steel | 1 | −11.3 | −49.8 | 4.4 | −12.3 |
| | | | | | 5.9 | 23.3 | 3.9 | 9.2 |
| B11 | | | | 2 | 11.1 | 42.1 | 4.5 | 18.4 |
| B12 | E14 | X | Wood | 4 | 6.1 | 32.6 | 5.3 | 29.0 |
| B13 | | | Steel | 2 | 5.1 | 42.0 | 8.3 | 17.2 |
| B14 | | Y | Wood | 1 | −4.6 | −26.0 | 5.7 | −10.8 |
| | | | | | 3.2 | 13.5 | 4.2 | 4.9 |
| B15 | | | Steel | 1 | −7.2 | −22.4 | 5.4 | −16.3 |
| | | | | | 1.4 | 15.5 | 11.0 | 6.4 |
| B16 | | Z | Wood | 2 | 1.3 | 5.7 | 4.3 | 6.5 |
| B17 | | | Steel | 1 | 3.6 | 23.6 | 6.6 | 18.8 |
| B18 | | XY | Wood | 1 | −11.3 | −38.6 | 3.4 | −9.2 |
| | | | | | 5.6 | 19.1 | 3.4 | 4.9 |
| B19 | | | Steel | 1 | −20 | −50 | 2.5 | −16.5 |
| | | | | | 6.8 | 24.3 | 3.6 | 9.9 |
| B20 | | | | 2 | −21.5 | −38.7 | 1.8 | −26.6 |

$V_y$ and $V_u$ in mm. $F_{max}$ in kN. Dir.: Direction. #: Number of brackets in the joint.

## References


[1] Andreasson S, Yasumura M, Daudeville L. Sensitivity study of the finite element model for wood-framed shear walls. J Wood Sci 2002:171–8.
[2] ASTM E 2126. Standard Test method for cyclic (reversed) load for shear resistance of vertical elements of the lateral force resisting systems for buildings. American Society for Testing and Materials (ASTM); 2007.
[3] Ayoub A. Seismic analysis of wood building structures. Eng Struct 2007;29:213–23.
[4] Boudaud C, Hameury S, Faye C, Daudeville L. European seismic design of shear walls: experimental and numerical tests and observations. World Conf Timber Eng Proc 2010.
[5] Ceccotti A, Karacabeyli E. Validation of seismic design parameters for wood-frame shear wall systems. Can J Civil Eng 2002;29:484–98.
[6] Ceccotti A, Vignoli A. A hysteretic behavioural model for semi-rigid joints. Eur Earthquake Eng 1989;3:3–9.
[7] Chui Y, Ni C, Jiang L. Finte-element model for nailed wood joints under reversed cyclic load. J Struct Eng 1998;124(1):96–103.
[8] Clough R. Effect of stiffness degradation on earthquake ductility requirements. Technical report No. SESM 66-16, University of California, Berkeley; 1966.
[9] Collins M, Kasal B, Paevere P, Foliente G. Three-dimensional model of light frame wood building. I: Model description. J Struct Eng 2005;131(4):676–83.
[10] Daudeville L, Davenne L, Yasumura M. Prediction of the load carrying capacity of bolted timber joints. Wood Sci Technol 1999:15–29.
[11] Dolan J. The dynamic response of timber shear walls. Ph.D. thesis, University of British Columbia, Vancouver, BC, Canada; 1989.
[12] EN 12329-1. Wood-based panels – characteristic values for structural design – Part 1: OSB, particleboards and fibreboards; 2002.
[13] EN 12512. Timber structures – test methods – cyclic testing of joints made with mechanical fasteners; 2002.
[14] EN 1995-1-1. Design of timber structures. Part 1-1: General – common rules and rules for buildings; 2005.
[15] EN 1998-1. Design of structures for earthquake resistance – general rules, seismic actions and rules for buildings; 2005.
[16] EN 338. Structural timber – strength classes; 2003.
[17] Folz B, Filiatrault A. Cyclic analysis of wood shear walls. J Struct Eng 2001;127(4):433–41.
[18] Folz B, Filiatrault A. Seismic analysis of woodframe structures. II: Model implementation and verification. J Struct Eng 2004;130(9):1361–70.
[19] Fonseca F, Rose S, Campbell S. Nail, wood screw, and staple fastener connections. Caltech wooframe project. Chapter: Testing setup; 2002.
[20] Foschi R. Analysis of wood diaphragms and trusses, Part 1: Diaphragms. Can J Civil Eng 1977;4(3):345–62.
[21] Girhammar U, Kallsner B. Elasto-plastic model for analysis of influence of imperfections on stiffness of fully anchored light-frame timber shear walls. Eng Struct 2009;31:2182–93.
[22] Gupta A, Kuo G. Behavior of wood-framed shear walls. J Struct Eng 1985;111(8):1722–33.
[23] Humbert J. Characterization of the behavior of timber structures with metal fasteners undergoing seismic loadings. Ph.D. thesis, Grenoble University; 2010.
[24] Johansen K. Theory of timber connections. Int Assoc Build Struct Eng 1949:249–62.
[25] Judd J. Analytical modeling of wood-frame shear walls and diaphragms. Master's thesis, Brigham Young University; 2005.
[26] Kallsner B, Girhammar U. Plastic models for analysis of fully anchoared light-framed timber shear walls. Eng Struct 2009;31:2171–81.
[27] Kasal B, Leichti R. Nonlinear finite-element model for light-frame stud walls. J Struct Eng 1992;118(11):3122–35.
[28] Kivell T, Moss P, Carr A. Hysteretic modelling of moment-resisting nailed timber joints. Bull. New Zealand Natl Soc Earthquake Eng 1981;14(4):233–43.
[29] Li M, Foschi R, Lam F. Modeling hysteretic behavior of wood shear walls with a protocol-independent nail connection algorithm. J Struct Eng 2012;138(1):99–108.
[30] Loo W, Quenneville P, Chouw N. A numerical study of the seismic behaviour of timber shear walls with slip-friction connectors. Eng Struct 2012;34:233–43.
[31] Malo K, Siem J, Ellingsbo P. Quantifying ductility in timber structures. Eng Struct 2011;33:2998–3006.
[32] Meghlat E, Oudjene M, Ait-Aider H, Batoz J. A new approach to model nailed and screwed timber joints using the finite element method. Construct Build Mater 2013;41:263–9.
[33] Meireles H, Bento R, Cattaro S, Lagomarsino S. A hysteretic model for frontal walls in pombalino buildings. Bull Earthquake Eng 2012.
[34] Munoz W, Mohammad M, Salenikovich A, Quenneville P. Determination of yield point and ductility of timber assemblies: in search for a harmonised approach. Engineering Wood Products Association; 2008.
[35] Oudjene M, Meghlat E, Ait-Aider H, Batoz J. Non-linear finite element modelling of the structural behaviour of screwed timber-to-concrete composite connections. Compos Struct 2013:102:20–28.
[36] Pang W, Rosowsky D. Beam-spring model for timber diaphragm and shear walls. Struct Build 2010;163(SB4):227–44.
[37] Pang W, Rosowsky D, Pei S, Lindt JVD. Evolutionary parameter hysteretic model. J Struct Eng 2007;133(8):1118–29.
[38] Richard N, Daudeville L, Prion H, Lam F. Timber shear walls with large openings: experimental and numerical prediction of the structural behaviour. Can J Civil Eng 2002:29:713–724.
[39] Saiidi M, Sozen M. Simple and complex models for nonlinear seismic response of reinforced concrete structures. Structural research series No. 466, Civil Engineering Studies, University of Illinois et Urbana-Champaign; 1979.
[40] Stewart W. The seismic design of plywood-sheathed shear walls. Ph.D. thesis, Univ. of Canterbury, Christchurch, New Zealand; 1987.
[41] Xu J, Dolan J. Development of a wood-frame shear wall model in abaqus. J Struct Eng 2009;135(8):977–84.
[42] Xu J, Dolan J. Development of nailed wood joint element in abaqus. J Struct Eng 2009;135(8):968–76.
[43] Yasumura M, Kamada T, Imura Y, Uesugi M, Daudeville L. Pseudodynamic tests and earthquake response analysis of timber structures ii: two-level conventional wooden structures with plywood sheathed shear walls. J Wood Sci 2006;52:69–74.